Micro- and nanoparticle generation during nanosecond laser ablation: correlation between mass and optical emissions

Santiago Palanco,[1,*] Salvatore Marino,[2] M. Gabás,[1] Shanti Bijani,[1] Luis Ayala,[1] and José R. Ramos-Barrado[1]

[1]*Dept. Física Aplicada I, The Nanotech Unit, University of Málaga, 29071 Málaga, Spain*
[2]*Dept. Fisica, Università della Calabria, IPCF-CNR UOS Cosenza, Ponte Pietro Bucci Cubo 33B 87036 Rende (CS), Italy*
[*]*spalanco@uma.es*

Abstract: The particulate emission during nanosecond ablation of gold targets was investigated at various fluences (10-100 Jcm^{-2}) and vacuum levels (0.05-750 Torr). Atomic emission spectra were acquired during the ablation process and post-mortem characterization of particle spatial distribution was performed using scanning electron microscopy. The discussion of the results in the context of existing theoretical models permitted the identification of four distinct mass removal mechanisms. While the presence, shape and intensity of atomic emission lines is a telltale of the nanoparticle formation process, the fluctuations of the emission signal over a number of laser shots was linked to the production of microscopic debris.

OCIS codes: (140.3440) Laser-induced breakdown; (160.4236) Nanomaterials; (300.2140) Emission.

References and links

1. J. C. Miller, "A brief story of laser ablation," AIP Conf. Proc. **288**, 619–622 (1993).
2. M. Baudelet and B. W. Smith, "The first years of laser-induced breakdown spectroscopy," J. Anal. At. Spectrom. **28**(5), 624–629 (2013).
3. R. E. Russo, X. Mao, J. J. Gonzalez, V. Zorba, and J. Yoo, "Laser ablation in analytical chemistry," Anal. Chem. **85**(13), 6162–6177 (2013).
4. W. M. Steen and J. Mazumder, *Laser Material Processing* (Springer, 2010).
5. A. V. Kabashin, P. Delaporte, A. Pereira, D. Grojo, R. Torres, T. Sarnet, and M. Sentis, "Nanofabrication with pulsed lasers," Nanoscale Res. Lett. **5**(3), 454–463 (2010).
6. J. Gonzalo, J. Siegel, A. Perea, D. Puerto, V. Resta, M. Galvan-Sosa, and C. N. Afonso, "Imaging self-sputtering and backscattering from the substrate during pulsed laser deposition of gold," Phys. Rev. B **76**(3), 035435 (2007).
7. J. Schou, "Physical aspects of the pulsed laser deposition technique: The stoichiometric transfer of material from target to film," Appl. Surf. Sci. **255**(10), 5191–5198 (2009).
8. S.-B. Wen, X. Mao, R. Greif, and R. E. Russo, "Experimental and theoretical studies of particle generation after laser ablation of copper with a background gas at atmospheric pressure," J. Appl. Phys. **101**(12), 123105 (2007).
9. S. Palanco and J. Laserna, "Spectral analysis of the acoustic emission of laser-produced plasmas," Appl. Opt. **42**(30), 6078–6084 (2003).
10. S. Conesa, S. Palanco, and J. J. Laserna, "Acoustic and optical emission during laser-induced plasma formation," Spectrochim. Acta, B At. Spectrosc. **59**(9), 1395–1401 (2004).
11. R. E. Russo, X. L. Mao, H. C. Liu, J. H. Yoo, and S. S. Mao, "Time-resolved plasma diagnostics and mass removal during single-pulse laser ablation," Appl. Phys., A Mater. Sci. Process. **69**(7), S887–S894 (1999).
12. M. Baudelet, L. Guyon, J. Yu, J. P. Wolf, T. Amodeo, E. Fréjafon, and P. Laloi, "Femtosecond time-resolved laser-induced breakdown spectroscopy for detection and identification of bacteria: A comparison to the nanosecond regime," J. Appl. Phys. **99**(8), 084701 (2006).
13. M. Baudelet, L. Guyon, J. Yu, J. P. Wolf, T. Amodeo, E. Fréjafon, and P. Laloi, "Spectral signature of native CN bonds for bacterium detection and identification using femtosecond laser-induced breakdown spectroscopy," Appl. Phys. Lett. **88**(6), 063901 (2006).
14. M. Weidman, K. Lim, M. Ramme, M. Durand, M. Baudelet, and M. Richardson, "Stand-off filament-induced ablation of gallium arsenide," Appl. Phys. Lett. **101**(3), 034101 (2012).

#200406 - $15.00 USD Received 1 Nov 2013; revised 13 Jan 2014; accepted 17 Jan 2014; published 13 Feb 2014

15. M. Lenzner, J. Krüger, S. Sartania, Z. Cheng, C. Spielmann, G. Mourou, W. Kautek, and F. Krausz, "Femtosecond optical breakdown in dielectrics," Phys. Rev. Lett. **80**(18), 4076–4079 (1998).
16. P. R. Willmott and J. R. Huber, "Pulsed laser vaporization and deposition," Rev. Mod. Phys. **72**(1), 315–328 (2000).
17. E. Lescoute, L. Hallo, D. Hébert, B. Chimier, B. Etchessahar, V. T. Tikhonchuk, J.-M. Chevalier, and P. Combis, "Experimental observations and modeling of nanoparticle formation in laser-produced expanding plasma," Phys. Plasmas **15**(6), 063507 (2008).
18. B. S. Luk'yanchuk, W. Marine, and S. I. Anisimov, "Condensation of vapor and nanoclusters formation within the vapor plume, produced by ns-laser ablation of Si," Laser Phys. **8**, 291–302 (1998).
19. P. M. Ossi, "Cluster synthesis and cluster-assembled deposition in nanosecond pulsed laser ablation," in *Laser-Surface Interactions for New Materials Production*, A. Miotello and P. M. Ossi, eds. (Springer, 2010).
20. *Laser-Induced Plasmas and Applications*, L. J. Radziemski and D. A. Cremers, eds. (Marcel Dekker, 1989).
21. R. E. Russo, X. Mao, J. H. Yoo, and J. Gonzalez, "Laser ablation," in *Laser-Induced Breakdown Spectroscopy*, S. N. Thakur and J. P. Singh, eds. (Elsevier, 2008).
22. J. Koch and D. Günther, "Review of the state-of-the-art of laser ablation inductively coupled plasma mass spectrometry," Appl. Spectrosc. **65**(5), 155–162 (2011).
23. X. Mao and R. E. Russo, "Observation of plasma shielding by measuring transmitted and reflected laser pulse temporal profiles," Appl. Phys., A Mater. Sci. Process. **64**, 1–6 (1997).
24. R. G. Root, "Modeling of post-breakdown phenomena," in *Laser-Induced Plasmas and Applications*, L. J. Radziemski and D. A. Cremers, eds. (Marcel Dekker, 1989).
25. A. K. Knight, N. L. Scherbarth, D. A. Cremers, and M. J. Ferris, "Characterization of laser-induced breakdown spectroscopy (LIBS) for application to space exploration," Appl. Spectrosc. **54**(3), 331–340 (2000).
26. H. R. Griem, *Plasma Spectroscopy* (McGraw-Hill, 1964).
27. C. Aragón and J. A. Aguilera, "Characterization of laser induced plasmas by optical emission spectroscopy: a review of experiments and methods," Spectrochim. Acta, B At. Spectrosc. **63**(9), 893–916 (2008).
28. D. Riley, I. Weaver, T. Morrow, M. J. Lamb, G. Martin, L. Doyle, A. Al-Khateeb, and C. L. S. Lewis, "Spectral simulation of laser ablated magnesium plasmas," Plasma Sour. Sci. Technol. **9**(3), 270–278 (2000).
29. A. Bogaerts, Z. Chen, R. Gijbels, and A. Vertes, "Laser ablation for analytical sampling: what can we learn from modeling?" Spectrochim. Acta, B At. Spectrosc. **58**(11), 1867–1893 (2003).
30. D. J. Lim, H. Ki, and J. Mazumder, "Mass removal modes in the laser ablation of silicon by a Q-switched diode-pumped solid-state laser (DPSSL)," J. Phys. D **39**(12), 2624–2635 (2006).
31. A. Gragossian, S. H. Tavassoli, and B. Shokri, "Laser ablation of aluminum from normal evaporation to phase explosion," J. Appl. Phys. **105**(10), 103304 (2009).
32. N. M. Bulgakova and A. V. Bulgakov, "Pulsed laser ablation of solids: transition from normal vaporization to phase explosion," Appl. Phys., A Mater. Sci. Process. **73**(2), 199–208 (2001).
33. M. Stafe, C. Negutu, and I. M. Popescu, "Theoretical determination of the ablation rate of metals in multiple-nanosecond laser pulses irradiation regime," Appl. Surf. Sci. **253**(15), 6353–6358 (2007).
34. Gwyddion software package V2.29, GNU General Public License, 2012, http://gwyddion.net
35. G. I. Taylor, "The formation of a blast wave by a very intense explosion. I. Theoretical discussion," Proc. R. Soc. London A Math. Phys. Sci. **201**(1065), 159–174 (1950).
36. G. I. Taylor, "The formation of a blast wave by a very intense explosion. II. The atomic explosion of 1945," Proc. R. Soc. London A Math. Phys. Sci. **201**(1065), 175–186 (1950).
37. L. I. Sedov, "Propagation of strong shock waves," J. Appl. Math. Mech. **10**, 241–250 (1946).

1. Introduction

The interaction of a laser pulse with a surface can lead to sudden local heating followed by a supersonic plasma expansion and the generation of particles in what has become to be known as laser ablation. Although the first papers on this phenomena date from the 1960s [1,2], it has found applications in a number of material processing and characterization techniques like laser welding, drilling, cutting, patterning, coating and optical and mass spectrometry, among many others [3–5]. A common point to all of these techniques is the need of controlling aerosol production. In some cases to avoid damage by the particles ejected to the processing optics, in others because the formation of micron-sized particles affects the analytical figures of merit, and in some instances owing to the impact that the particle size distribution or stoichiometry might have on the quality of a certain product [6,7].

In general, the products of laser ablation appear as a distribution of particles of different nature and morphology whose size spans seven orders of magnitude (10^{-10}-10^{-3} m), ranging from ions/atoms, to nanoparticles, and micron- and millimeter-sized particles. This sentence alone should suffice to state the complexity of laser ablation but it is worth noting that 50 years on, the physical and chemical processes involved are not fully understood [8–10].

A number of works has been devoted to picosecond and femtosecond laser ablation and its applications [11–14]. In the femtosecond time domain, coupling of the laser energy to the

#200406 - $15.00 USD Received 1 Nov 2013; revised 13 Jan 2014; accepted 17 Jan 2014; published 13 Feb 2014

sample is significantly shorter than heat diffusion and the hydrodynamic time scale and interactions of the incoming light pulse with the expanding material are avoided, what is of particular interest for the study of debris production [15–17]. In contrast, nanosecond laser ablation is prone to the production of undesired ejecta. Along with a expanding cloud composed by plasma and/or vapor, an aerosol of molten or solid material is often ejected from the target surface [18–22]. The volume fraction of molten mass can be reduced by increasing the pulse energy per unit mass although it cannot be entirely neglected as a consequence of plasma interaction with the surface and with the nanosecond pulse tail [23].

Product-wise, it is widely accepted that femtosecond laser ablation is the way to go but, beyond nanoparticles, there is a huge number of applications, laboratories and commercial systems which for reasons of simplicity, reliability or cost use nanosecond laser sources. To name one, it has taken a whole new generation of fiber lasers to see the first commercial femtosecond laser ablation inductively-coupled plasma mass spectrometer.

In this paper, we have centered our investigation on the nanosecond laser ablation of gold. Our main purpose is gaining a better insight on the mechanisms involved in laser ablation in order to reduce or control the presence of microscopic particulate debris which, in turn, may help to improve the efficiency and reproducibility of the vaporization process and the atomic emission. To this end, measurements from time-resolved optical emission along with post-mortem analysis of the targets and of the spatial and size distributions of the particles have been carried out under the experimental conditions commonly used in nanosecond ablation applications.

2. Experimental section

A schematic of the experimental arrangement is shown in Fig. 1(a). A custom-made chamber (Trinos Vacuum-Projects, S.L.) served as the sample cell for this investigation. The chamber top was covered with a transparent PMMA lid which allowed direct observation of the sample inside. Two of the side ports were fitted with AR coated BK7 windows used to admit the 1064 nm ablation laser beam and for a rolling shutter CMOS camera (UI-1240SE-M-GL, IDS) which was alternated with an EM-CCD camera (iXon DU860E, Andor Technology) used to capture images of the plasma. The chamber was fitted with ancillaries to allow controlled gas flow and pressure operation. The fundamental output of a Q-switched Nd:YAG laser (Quantel Brilliant B) with a maximum energy of 850 mJ per 6-ns pulse was focused at a 10 Hz repetition rate into the center of the chamber where the sample was placed in a vertical position and normal to the incident ablation beam. In order to allow tighter focusing, the laser beam was expanded with a magnification factor of 4 and then focused into the sample chamber with an AR-coated BK7 positive aspheric lens (f = 150 mm). The optical emission from the laser-induced plume was collected with a fused silica lens (f = 250 mm, d = 75 mm) which focused the light to the entrance slit of a f/3.6, 163 mm focal length Czerny-Turner spectrograph (Andor SR163i) fitted with a 1200 line/mm grating and a 2048x512 pixel ICCD detector (Andor iStar DH720-18F-03). Synchronization of the laser source and detection was carried out with a digital delay and pulse generator (Stanford Research Systems DG535) in combination with the internal delay generator of the ICCD.

High purity (99.99%) gold foil samples 127 μm in thickness (Sigma-Aldrich) were irradiated with the fundamental wavelength of the Nd:YAG laser at 10 Hz until they were fully drilled by the repeated action of the laser over the same spot. The ambient air pressure ranged from 0.05 Torr to 750 Torr and was kept constant over each ablation cycle. As shown in Fig. 1(b), the gold samples were mechanically fastened to a thick copper plate which was used as sample holder and, additionally, served both as a heat sink and as a spectral flag of the full drilling of the gold sample. In this way, the amount of material removed per ablation cycle amounted closely to the full 127 μm of the sample thickness regardless the number of laser pulses required to get through. The use of a thin sample substantially reduces plasma interaction with the crater walls and permits a more representative estimation of the average ablation rate (*AAR*). The particulate emission ejected during each ablation cycle was collected in pairs of silicon witness plates (WP) placed horizontally below the incoming laser beam

#200406 - $15.00 USD Received 1 Nov 2013; revised 13 Jan 2014; accepted 17 Jan 2014; published 13 Feb 2014

axis and perpendicular to the gold sample. Using two separate WP per ablation cycle provided information on the spatial distribution of the particles ejected.

An atomic emission spectrum was acquired per each laser shot. All spectra registered covered the 225-315 nm spectral region where both Au and Cu atomic emission are present. A delay of 1.5 μs from the laser pulse was applied to all acquisitions to reduce the contribution from the characteristic continuum background. The integration gate was 50 ns. Since the plasma volume grew from 1 to 2 mm in diameter at 750 Torr to about 80 mm at 0.05 Torr, care was taken to collect the photons emitted from the majority of the region the plasma expands to at low pressure.

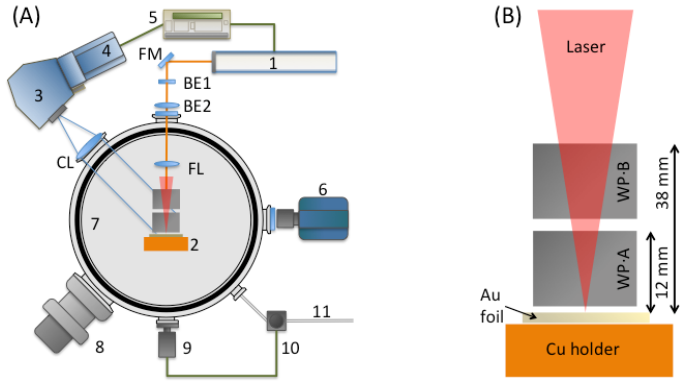

Fig. 1. (A) Top view of the experimental setup. 1 laser source, 2 sample holder, 3 spectrograph, 4 iCCD, 5 digital delay generator, 6 CMOS/EMCCD, 7 vacuum chamber, 8 turbo-molecular pump, 9 baratron, 10 pulsed valve, 11 gas inlet, FM folding mirror, BE1, BE2 beam expander components, FL focusing lens, CL collection lens. (B) layout of the sample holder illustrating the gold sample, the laser beam direction and the two witness plates WP-A and WP-B.

3. Results and discussion

3.1 Atomic emission spectra

Along with laser fluence, ambient pressure is possibly the parameter with the largest influence in laser ablation. Figure 2 compares the spectral emission of a gold sample irradiated with two different fluences (10 and 100 J cm^{-2}) under two ambient air pressures (750 and 0.5 Torr) each. At a first glance, there are noticeable differences between the spectra at atmospheric pressure and these at 0.5 Torr that evidence the impact of switching the operating pressure. While the two spectra acquired under atmospheric pressure are rich in both Au(I) and Au(II) emission lines and the broad continuum contribution is still noticeable, the flat baselines of the spectra obtained under vacuum conditions show no trace of the bremsstrahlung radiation and the atomic emission is less intense, less profuse in lines and with an apparently smaller aspect ratio. A closer look to the emission lines in spectra (c) and (d) reveals that all of them correspond to Au(I) transitions and are actually self-absorbed, implying the existence of a region in the line of sight between the Au(I) emitters and the detector where colder Au(I) absorbs line radiation. Both self-absorption and the absence of Au(II) emission are indicative of an overall decrease in plasma temperature, what is in good agreement with the calculations in [18] which predicts a low-temperature vapor-composed plume in which nanoparticles are formed as a result of collisions.

#200406 - $15.00 USD Received 1 Nov 2013; revised 13 Jan 2014; accepted 17 Jan 2014; published 13 Feb 2014

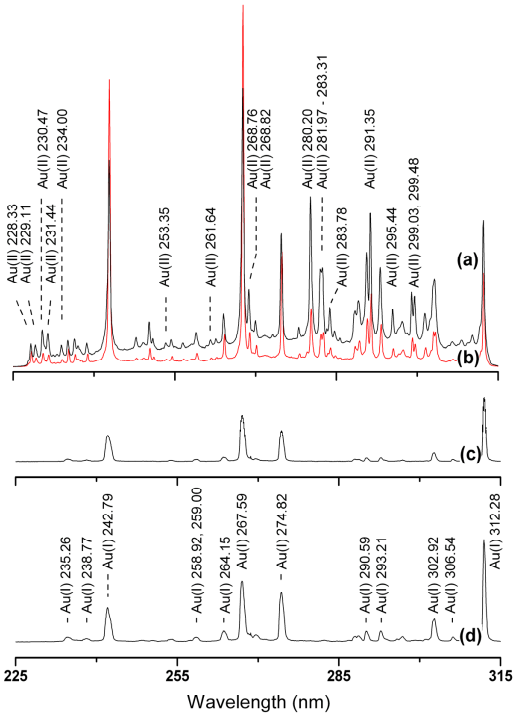

Fig. 2. Atomic emission spectra of a gold sample acquired at different fluence and vacuum conditions: (a) 100 J cm^{-2} and 750 Torr, (b) 10 J cm^{-2} and 750 Torr, (c) 100 J cm^{-2} and 0.5 Torr, (d) 10 J cm^{-2} and 0.5 Torr. The acquisition gate was 50 ns after a delay of 1500 ns from the laser pulse. The intensity (a.u.) scales of spectra (c) and (d) has been magnified 3.7 times to improve visibility. Wavelength labels have been rounded to two decimal places.

The situation in spectra (a) and (b) is the opposite to that described for (c) and (d). In particular, for the same energy input as spectrum (c), the noticeable continuum and the abundance of broadened atomic and ionic lines found in (a) are a clear signal of higher plasma temperatures. However this is not necessarily indicative of a more efficient coupling of the laser energy to the sample. The plasma in (a), at 100 J cm^{-2} and atmospheric pressure, progresses as a laser supported radiation wave (LSR) in which the fast expansion and intense continuum radiation emitted by the plasma raise the temperature of the ambient gas to a level at which it absorbs the laser radiation through inverse bremsstrahlung and becomes ionized. Therefore, the interaction between laser and plasma shifts ahead of the shock wave front, detaching from the target surface which becomes shielded from the incoming beam [24]. Spectrum (b) is a further confirmation of the latter reasoning. Lowering the fluence dose to 10 J cm^{-2} yielded up to ~40% higher emission intensities with thinner lines and a lower continuum contribution.

3.2 Atomic emission vs particle ejection

The signal corresponding to the Au(I) line at 264.148 nm was registered and plotted versus pressure between 0.05 and 750 Torr. This particular line was selected over other stronger ones with high transition probabilities, like Au(I) at 267.595 nm, in order to reduce the contribution of self-absorption. The results in Fig. 3 show that the signal decreases monotonically with the vacuum level. This behavior is different from that observed by other researchers [25] and from our own observations for the laser ignition of Ar gas, plotted in the inset of Fig. 3, which exhibits a maximum for pressures slightly below atmospheric. The increase in the Ar(I) 696.543 signal not only proved the validity of the optical collection arrangement at low pressure but also stressed the apparently anomalous behavior of the Au(I)

#200406 - $15.00 USD Received 1 Nov 2013; revised 13 Jan 2014; accepted 17 Jan 2014; published 13 Feb 2014

emission. In order to shed light into this, the ablated mass per pulse (*AAR*) was estimated from the number of laser shots required to drill the 127 μm gold foil. The results are plotted in Fig. 4 and illustrate that the *AAR* increases with decreasing pressure, which is consistent with the decline of plasma shielding with vacuum already discussed for the spectra in Figs. 2(c) and 2(d). However, the increase of the *AAR* under vacuum may appear to be in contradiction with the decreasing trend exhibited by the atomic emission in Fig. 3. Assuming an optically thin plasma under local thermodynamic equilibrium, the integrated intensity I_λ, for a particular transition with wavelength λ, of a species in the plasma, is determined by [26,27]:

$$I_\lambda = \frac{hc}{\lambda} gAN \frac{e^{-E/kT}}{Q(T)} \quad (1)$$

where h is the Planck's constant, c is the speed of light, g is the degeneracy of the upper level of the transition, A is the transition probability, N is the number density of the species undergoing the transition, k is the Boltzmann's constant and Q is the partition function.

According to Eq. (1), and given the negligible presence of Au(II) and higher ionization states, the decrease of the Au(I) intensity in Fig. 3 could be motivated by the low plasma temperature or by a decrease in the number of emitters. Even if the decrease of the plasma temperature with vacuum is patent, the substantial increase in the *AAR* does not seem to agree with the number of emitters, i.e. there is a deficit of emitters as compared to the *AAR* measured even if the effect of self-absorption was compensated for [28].

In addition, a larger number of emitters would improve the Au(I) signal-to-noise ratio proportionally to the square root of the number of emitters. But far from decreasing, the relative standard deviation (*RSD* = 100/*SNR*) of the atomic emission signal increases from approximately 4.5% at 750 Torr to 17% at 0.5 Torr, which suggests that the signal could be affected by excess noise arising mainly from the shot-to-shot fluctuations in the mass ablated.

In any case, the condensation of micrograms of Au atoms would require an unrealistically high number of collisions to occur in the expanding plume [29] and, more importantly, a rough estimation of the energy required to evaporate the 21.9 μg pulse^{-1} of Au (the *AAR* at 0.5 Torr) yields 3.4 J, far from the 0.8 J available (it even fails to explain the 1.6 J required for the *AAR* measured at 750 Torr). These facts rule out evaporation as the only ablation mechanism and points towards the random formation of larger (sub-micrometer and micrometer sized) particles through a less energy-demanding path.

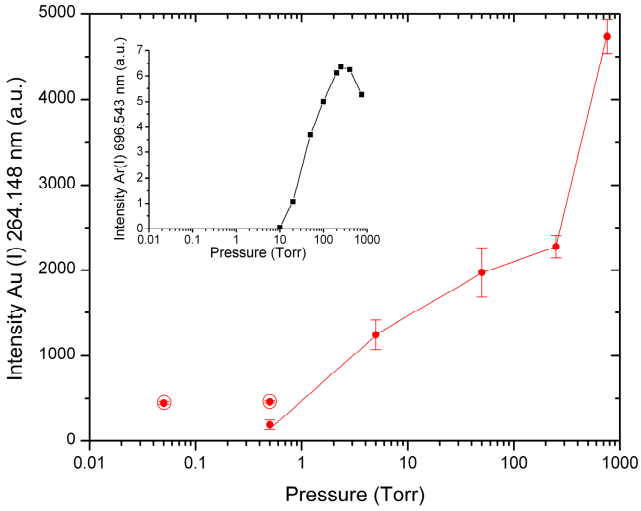

Fig. 3. Intensity of the Au(I) emission line at 264.148 nm versus pressure. (solid dot) 100 J cm^{-2}, (circled dot) 10 J cm^{-2}. The error bars correspond to the standard deviation of the line intensity over 50 successive laser shots on the same surface spot. The inset illustrates the intensity of the Ar(I) 696.543 nm line in the same pressure interval.

#200406 - $15.00 USD Received 1 Nov 2013; revised 13 Jan 2014; accepted 17 Jan 2014; published 13 Feb 2014

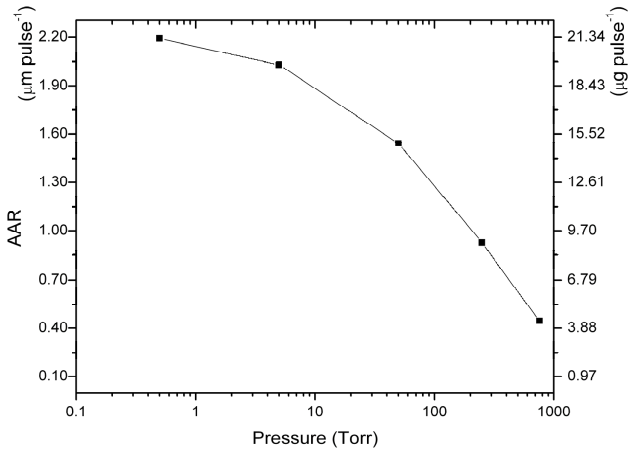

Fig. 4. Averaged ablation rate (*AAR*) calculated by counting the number of laser shots required to drill a 127-μm thick gold foil in the 0.5-750 Torr interval.

3.3 Particle splashing

Besides condensation, there are three additional mechanisms responsible for particle production during laser ablation: phase explosion, recoil ejection, and exfoliation. The first two are also known as splashing and can produce droplets of molten material, while the third mechanism -know as exfoliation- is responsible for particulate ejection by recurring melting-solidification cycles of a sample surface layer until the outgrowths get detached and ejected as irregular particles of many microns [16]. Phase explosion, also known as explosive boiling, is dominant in nanosecond laser ablation, specially of materials with a high thermal conductivity and low melting points like gold [30–32]. In recoil ejection, a thin melt layer between the expanding plasma and the solid bulk can be ejected as the melt is squeezed onto the solid bulk by the recoil pressure. Coincidentally, the size and morphology of the ejecta caused by this phenomena are analogous to those in explosive boiling, with the only difference in their angular distributions, which in recoil ejection has more of a crown form than that in explosive boiling [32,33]. It is worth noting that particles produced by splashing mechanisms are considered as debris in many applications.

3.4 Post-mortem analysis

In order to confirm that the mass deficit was due to splashing and to discern the particle production mechanism, an analysis of the size and spatial distribution of the ejected particles was conducted. Samples of the particles ejected during the spectral acquisitions of the previous section were collected in pairs of Si witness plates (WP) placed as described in the Experimental section. Figure 5 illustrates ten SEM micrographs of the WP. At low magnification, most WP reveal an unevenly gold-coated surface on top of which micron-sized particles stand out. Elemental analysis carried out with EDS detected solely Au and Si in the 93.7% of the sites probed -the remaining sites showed Cu contamination below 1%. Au-particle size and number was measured from micrographs at various magnifications with Gwyddion software package [34] and revealed a distribution of virtually round particles that ranged from a few nm to ~50 μm in diameter depending on the ablation pressure and position of the particular WP measured.

A trend which is apparent in the micrographs is that large particles (10-40 μm) seem to shift from WP-A at 750 Torr to both WP-A and WP-B at 250 Torr, and mainly to WP-B at 70 and 5 Torr. This increase in particle flight range is also true for the smaller particles as confirmed with the software and could be understood on the basis of the higher plume expansion velocities reached at decreasing pressures as per the previous discussions for Figs. 2–4. On the other side, even though a specific particle size was not characteristic at any

#200406 - $15.00 USD Received 1 Nov 2013; revised 13 Jan 2014; accepted 17 Jan 2014; published 13 Feb 2014

of the pressures mentioned, the overall volume of particles captured within the solid angle of both WP correlated, within reason, with the *AAR* in Fig. 4, supporting the possibility of splashing as the mass removal phenomena responsible for the decreased atomization and optical emission. Yet, it is remarkable, that the finding of a small number irregularly shaped particles in the WP between 750 and 5 Torr suggests that spallation -particles ejected in the solid phase from the surface- might have occurred occasionally as a consequence of phase explosion versus recoil ejection.

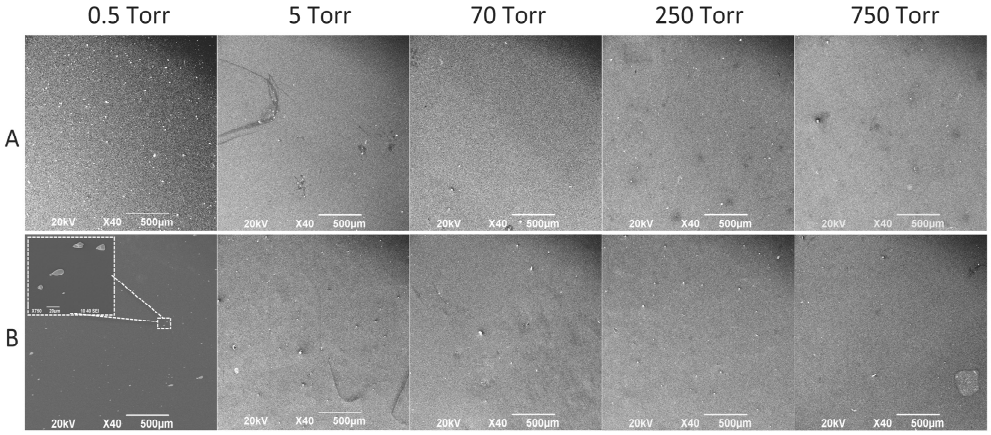

Fig. 5. Scanning electron micrographs of the WP used to collect the particle emission during irradiation of the gold samples with a 100 J cm^{-2} fluence. A, and B stand for the positions described for the WP in Fig. 1(b).

So far, the discussion has skipped the two micrographs at 0.5 Torr. The size distribution measured was narrower and particles smaller than 1 μm were almost absent at this pressure. This circumstance along with a larger particle count -the highest *AAR* was found at 0.5 Torr- contribute to the grainier look that WP-A at 0.5 Torr displays as compared to those at higher pressures. However, the particle fight range at 0.5 Torr was the shortest of the series, breaking the trend observed across the 5-750 Torr interval. This behavior could be attributed to the additional energy coupled to the sample, less shielded by the plasma at 0.5 Torr. The stronger recoil would squeeze the melt to flow at a large angle with the plasma expansion axis, leading to an increased preponderance of corona-like ejection mainly towards WP-A. Indeed, WP-B mostly exhibits the original dark silicon background with the only presence of isolated gold splashes which did not solidify in-flight and landed in a liquid form. This could be explained by the increased expansion velocity of the plasma at 0.5 Torr as predicted by the scaling for a blast explosion [35–37] following the instantaneous release of an energy, *E*. Equation (2) describes the position, *R*, as a function of time, *t*, for a shock wave front with spherical propagation ($\beta = 3$) in a gas with density, ρ. λ is a constant.

$$R = \lambda \left(\frac{E}{\rho} \right)^{1/(2+\beta)} t^{2/(2+\beta)} \tag{2}$$

In the worst case scenario, i.e. assuming no increase in the energy effectively coupled, a ten-fold pressure drop from 5 to 0.5 Torr would amount to a 60% faster expansion velocity, according to Eq. (2). Such an increase in the expansion velocity, along with the decrease in the collision probability, could be linked to the drastic reduction in the number of nanoparticles found at this pressure.

3.5 Nearly debris-free ablation

Lowering the fluence by one order of magnitude to 10 Jcm^{-2} while keeping the pressure at 0.5 Torr -i.e. the same E/ρ ratio as for the 5 Torr, 100 Jcm^{-2} sample- increased the presence of

#200406 - $15.00 USD Received 1 Nov 2013; revised 13 Jan 2014; accepted 17 Jan 2014; published 13 Feb 2014

nanoparticles but, more importantly, the *AAR* fell abruptly to 121 ng pulse^{-1} what resulted in a significantly lower 3% atomic emission RSD as compared to the slight increase of the signal shown by the circled dots in Fig. 3.

4. Conclusion

Three conclusions can be drawn from the above results and discussions: (i) plasma shielding can be limiting factor even with an operating pressure of 0.5 Torr. (ii) The various particle production mechanisms discussed are relevant and compete against each other. The prevalence of a particular mechanism depends on the experimental conditions used with a given material. (iii) Atomic emission spectroscopy can be used as a real time telltale of the ablation phenomena for nanoparticle production, and even if an optically dense plasma could lead to inaccurate quantitative measurements, valid semiquantitative results have been inferred from the spectra acquired during the ablation process. A single spectrum, whether averaged from multiple laser shots or corresponding to a single shot, can be used to infer the ionization degree or the plasma temperature. The presence and the intensity of atomic emission lines is a direct measurement of the evaporated material which can be of interest for nanoparticle synthesis. The fluctuation of the emission over a number of laser shots has been linked with the formation of debris

The results obtained for gold are extensible to other metals with comparable thermal conductivity and melting point, and could be relevant for laser ablation based techniques like pulsed laser deposition, laser-induced breakdown spectroscopy, laser-ablation-inductively-coupled plasma followed by atomic emission spectrometry or mass spectrometry (PLD, LIBS, LA-ICP-AES, LA-ICP-MS, respectively).

Acknowledgments

This work has been partially funded by Ministerio de Economía y Competitividad program TEC2011-28639-C02-02. S.P. acknowledges the support of Ministerio de Ciencia e Innovación for a Ramón y Cajal fellowship. S.M. acknowledges the support of Regione Calabria (Italy) for a postdoctoral fellowship.

#200406 - $15.00 USD Received 1 Nov 2013; revised 13 Jan 2014; accepted 17 Jan 2014; published 13 Feb 2014